PCCP

Mechanisms for hydrogen evolution on transition metal phosphide catalysts and a comparison to Pt(111)

Journal:	*Physical Chemistry Chemical Physics*
Manuscript ID	CP-ART-09-2019-005094.R1
Article Type:	Paper
Date Submitted by the Author:	18-Oct-2019
Complete List of Authors:	Li, Chenyang; Johns Hopkins University Gao, Hao; Johns Hopkins University Wan, Wan; Johns Hopkins University Mueller, Tim; Johns Hopkins University,

Mechanisms for Hydrogen Evolution on Transition Metal Phosphide Catalysts and a Comparison to Pt(111) †

Chenyang Li,[1] Hao Gao,[1] Wan Wan,[1] and Tim Mueller,[1,*]

[1]Department of Materials Science and Engineering, Johns Hopkins University, Baltimore, Maryland 21218, United States

[*]Email: tmueller@jhu.edu

†Electronic supplementary information (ESI) available.

Abstract

Earth-abundant transition metal phosphides have been demonstrated to be promising alternative catalysts to replace Pt for hydrogen evolution reaction (HER). However, the mechanism for the hydrogen evolution reaction on transition metal phosphides remain unclear. Here we explore the catalytically active sites and the reaction mechanisms on a variety of model transition metal phosphide surfaces by building cluster expansion models and running Monte Carlo simulations. We demonstrate that the effect of hydrogen coverage, interaction between hydrogen atoms and desorption kinetics all dictate to the HER mechanisms and the active sites, and we propose mechanisms that are in good agreement with experimental studies. The present method provides a general and effective way to probe the active sites and study the mechanisms of catalytic reactions, which can facilitate rational design of highly active electrocatalysts.

Introduction

The hydrogen evolution reaction (HER) constitutes half of the water splitting reaction, which could produce H_2 from renewable energy resources and therefore reduce the demand for fossil fuels. In acid electrolytes protons are reduced to H_2 via $2H^+ + 2e^- \rightarrow H_2(g)$. Pt is one of the most active catalysts for this reaction,[1, 2] but there is great interest in finding alternative catalysts that do not depend on expensive metals. Transition metal phosphides have emerged from both experimental and theoretical studies as active HER catalysts with good performance and stability.[3-12] As these phosphides are made from earth-abundant materials, they have the potential to be more economically viable than Pt-based catalysts.

It has been shown that the hydrogen adsorption free energy ΔG_H (more negative values indicate stronger adsorption) is a suitable descriptor of the catalytic activity for HER, and typically an adsorption free energy around 0 eV demonstrates higher activity.[2, 13, 14] Although computational studies have shown that ΔG_H is near zero on some sites on model transition metal phosphide surfaces, the HER activity of these materials still remains below that of Pt.[2-8, 14-16] The hydrogen adsorption energy on transition metal phosphides has a strong coverage dependence compared to metals (e.g. ranging up to ~0.8 eV for Fe_2P), and the differences in ΔG_H between different sites on transition metal phosphide surfaces are large.[3, 7] Moreover, on pure metal catalysts the hydrogen coverage can reach almost a full monolayer at small overpotentials, whereas on metal phosphides and sulfides, the hydrogen surface coverages are much lower.[17-19] From a mechanistic point of view, it has been observed that the Tafel slopes for transition metal phosphides, a measure of how the log of the current changes with applied potential, are typically around 40~60 mV/dec, whereas

that of Pt is around 30 mV/dec.[4, 5, 9-11, 20] Taken together, these observations suggest that the mechanism of the HER on transition metal phosphides is significantly different from that on Pt.

To better understand the HER mechanisms on transition metal phosphide surfaces and how they compare to Pt, we have used the cluster expansion approach[21, 22] to model realistic arrangements of adsorbed hydrogen on transition metal phosphide and platinum surfaces. The cluster expansion is able to rapidly predict the energy of a particular arrangement of adsorbates on the surface of a material with high accuracy (typically within 5 meV / site compared to density functional theory[23]) while fully accounting for interactions between adsorbates. For these reasons, there has been increasing interest in using cluster expansions to study heterogeneous catalysis including surfaces and nanoparticles.[24-37] Here we have constructed cluster expansions on four model transition metal phosphide surfaces (FeP(011), Fe_2P(100), CoP(101), and Co_2P(101)) as well as the Pt(111) surface for comparison. Using these cluster expansions, we have determined hydrogen coverage and atomic order as a function of temperature and applied potential by running grand canonical Monte Carlo[38] simulations, and further understood how the coverage effects and interactions between atoms influence the active sites, their catalytic activities, and HER mechanisms.

Methodology

DFT. Density functional theory (DFT)[23] calculations were performed with the Vienna Ab initio Simulation Package (VASP),[39] in which the Kohn-Sham equations are solved by self-consistent algorithms. The revised Perdew-Burke-Ernzerhof (RPBE)[40, 41] exchange-correlation functional was used for all DFT calculations, and spin polarization was enabled. The Co, Fe, P, H_GW, Pt_pv

PBE projector-augmented wave (PAW)[42] potentials were used and all calculations were run with accurate precision to ensure that there were no wrap-around errors. For calculations with transition metal phosphides, the slab thickness and vacuum thickness were at least 10 Å and 15 Å, respectively. The Brillouin zone was sampled using efficient grids generated by the *k*-point grid server[43] with a minimum distance of 18 Å between real-space lattice points; For Pt(111), a minimum distance of 40 Å was used. The shift vectors were automatically chosen to minimize the number of irreducible *k*-points, and the grids were automatically optimized for slab calculations. The convergence criteria for the self-consistent iteration and the ionic relaxation loop were set to 10^{-4} eV and 10^{-3} eV per cell, respectively. Activation energies of elementary reaction steps were calculated using the climbing image nudged elastic band (CI-NEB) method.[44, 45] More details are provided in the Supplementary Information.

Cluster expansion. Cluster expansions are generalized Ising models[21, 22] that account for many-body interactions. Here, we have used cluster expansions to model the hydrogen adsorption on transition metal phosphide and platinum surfaces, where each possible adsorption site can exist in one of two states: occupied by hydrogen or vacant. We have used a Bayesian method[46] to fit the cluster expansion to sets of DFT training data, which has been shown to greatly improve the predictive accuracy of the cluster expansion for a given training set size.[27, 34, 46] The training set includes structures with varying hydrogen coverages (0~1 ML) and supercell sizes, allowing us to use a training set of small-size supercells to construct a cluster expansion that can be used to rapidly predict the energies and atomic orders of large-size supercells as a function of temperature and applied potential. More details on the construction of the cluster expansions are provided in the Supplementary Information.

Hydrogen coverage and evolution rates. We estimate the rate of hydrogen evolution by:

$$k = \nu \exp(-E_a / k_B T), \quad (1)$$

where E_a is the activation energy for H_2 formation and ν is a kinetic pre-factor. We assume the prefactor is the same for all reactions and express all current relative to that of the Tafel reaction on Pt at –0.12 V, which has the highest current of any reaction considered here. Since it is straightforward to calculate adsorption energies (ΔE) from cluster expansions but expensive to calculate activation barriers for all possible configurations, we have used Brønsted-Evans-Polanyi (BEP) relations[47-49] to estimate E_a for the Tafel and Heyrovsky steps, which were found to be rate-limiting. The constant-potential Heyrovsky barriers were calculated using the charge extrapolation scheme[50] (see Supplementary Information). The BEP relations were obtained by fitting a set of DFT-calculated E_a values to calculated adsorption energies on phosphides and Pt (Figure S4-S5). In this model the barrier does not change with respect to applied potential if we assume the Tafel mechanism is rate limiting, but changes linearly with respect to applied potential if the Heyrovsky mechanism is rate limiting, i.e., $E_a(U) = E_a(0) - \alpha e U$, where α is the charge transfer coefficient. The charge transfer coefficients are calculated for representative sites for each element using the supercell extrapolation scheme[17, 51] (see Figure S6 for more details). We found that across different materials the same elements had similar charge transfer coefficients; thus for simplicity we used the same charge transfer coefficients for Co and P sites on CoP and Co_2P. The hydrogen desorption rate is converted to current density by:

$$j = keN / A, \quad (2)$$

where N / A is the number of adsorption sites per area. The average current on the catalytic surface is calculated by summing up the current j contributed from all possible adsorbed hydrogen atoms (or pairs) and divided by the number of adsorption sites. Turnover frequencies on individual sites are calculated in a similar way.

Thermodynamically averaged currents, coverage, and arrangements of hydrogen atoms on different surfaces at different applied potentials were calculated using Metropolis Monte Carlo[38] simulations at 300 K. In these simulations we have accounted for the applied potential by using the computational hydrogen electrode (CHE)[52] model, in which we set the chemical potential of the proton-electron pair equal to half that of H_2(g):

$$\mu(H^+ + e^-) = \frac{1}{2}\mu(H_2) - eU, \tag{3}$$

where e is the elementary charge of an electron and U is the applied potential vs. the reversible hydrogen electrode (RHE). (In this paper, all listed potential values are vs. the RHE.) According to Skúlason *et al.*,[17, 53] the activation barrier for the proton-electron transfer to the surface of Pt (the Volmer step) is much lower than that of H_2(g) desorption, i.e. H_2(g) desorption would be the rate-limiting step for the HER. We have verified this is true for transition metal phosphides as well (Table S2) by computing the activation barriers using the charge extrapolation scheme, as detailed by Chan and Nørskov.[50] The chemical potential of adsorbed hydrogen can therefore be expected to be primarily determined by that of the proton-electron pair rather than by that of H_2. Thus the reference chemical potential when calculating the potential-dependent hydrogen coverage in Monte Carlo simulations was chosen to be $\mu(H^+ + e^-)$.

Results and Discussion

The surfaces studied in this paper, including the four transition metal phosphide surfaces and Pt(111), are shown in Figure 1. The terminations of the transition metal phosphide are those that are believed to be the most probable surfaces based on previous work by Kibsgaard *et al.*[3], but we note that it is possible that there are lower energy terminations or surface reconstructions. To construct the cluster expansions we identified possible hydrogen adsorption sites on each surface; these sites are also shown in Figure 1. Each of the cluster expansions was generated and fit using the Bayesian method,[46] resulting in leave-one-out cross-validation (LOO CV) errors, which are estimates of the prediction error, of 3.4, 7.4, 7.0, 4.3, and 6.6 meV / site for $Co_2P(101)$, CoP(101), $Fe_2P(100)$, FeP(011), and Pt(111) respectively. The cluster expansions were refined by adding newly predicted ground-state structures to the training sets until they were well-converged.

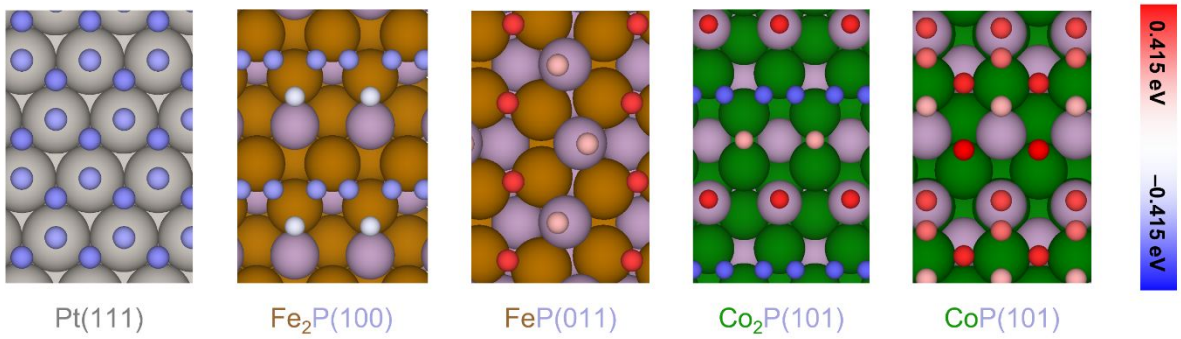

Figure 1. Surfaces with all possible hydrogen adsorption sites for Pt, Fe_2P, FeP, Co_2P, and CoP. Large grey spheres represent Pt, purple spheres represent P, gold spheres represent Fe, and green spheres represent Co. Small colored spheres represent H, and the colors indicate the free energy of adsorption ΔG_H for an isolated hydrogen atom at each site at a potential of 0 V.

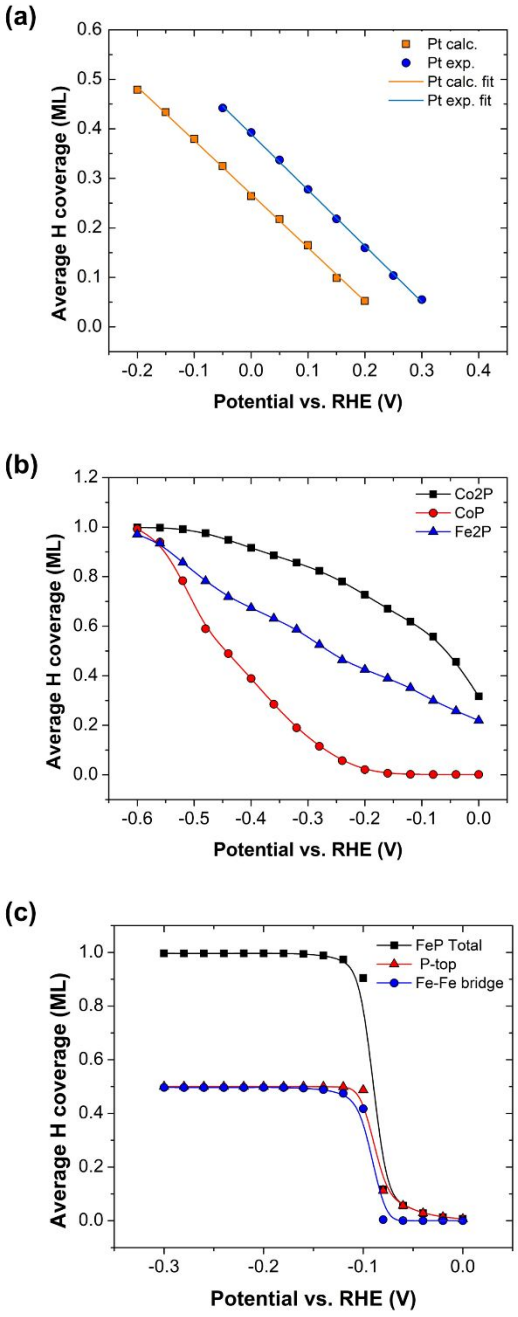

Figure 2. Average hydrogen coverage as a function of applied potential on (a) Pt(111), (b) the model surfaces for Co_2P, CoP, and Fe_2P. (c) Average hydrogen coverage and breakdown of the site contributions on FeP. The experimental data for Pt are taken from Markovic *et al.*[54] Note that the maximum coverage is 1 ML, so for Pt(111) a coverage of 0.5 ML means all fcc sites are filled.

We have used density functional theory to directly calculate hydrogen adsorption energies for isolated hydrogen atoms on each of the identified hydrogen adsorption sites (Figure 1). Hydrogen adsorption is generally stronger on the metal-bridge sites of Fe_2P/Co_2P than FeP/CoP. In contrast, hydrogen adsorption on P sites of FeP/CoP is stronger than that on Fe_2P/Co_2P. On Pt(111), hydrogen adsorption on the fcc site is 0.04 eV stronger than on the top site and all ΔG_H are slightly negative. We also considered the hcp site on Pt(111) and found that the hydrogen adsorption energy is the weakest among all three adsorption sites (~0.05 eV weaker than fcc). Thus we only include the fcc and top sites in the current model.

We examined the thermodynamically averaged surface hydrogen coverage as the applied potential is decreased (Figure 2a-c). The potential dependence of hydrogen coverage can be fit to a Frumkin isotherm:[54, 55]

$$\frac{\theta}{1-\theta}\exp\left(\frac{r\theta}{RT}\right)=\exp\left(-\frac{U_{RHE}F}{RT}\right)\exp\left(-\frac{\Delta G_H^{\theta=0}}{RT}\right) \quad (4)$$

where U_{RHE} is the applied potential, F is the Faraday constant, and ΔG_H is the free energy of adsorption, and r is the interaction parameter that characterizes the lateral interactions among adsorbed hydrogen atoms. The interaction parameter, which is related to the slope of the coverage with respect to applied potential, is repulsive for $r>0$ and attractive for $r<0$. On Pt(111), the value of the interaction parameter that fits best to the Monte Carlo simulations is 32 kJ/mol, which is in excellent agreement with experimentally measured value of 30 kJ/mol (Figure 2a).[54] The hydrogen coverage reaches 0.5 ML, corresponding to all fcc sites being filled, at about –0.16 V, which is shifted by about 0.1 V from experimental findings.[1, 54] The relative position of the curve is determined by the free energy of adsorption, where the small deviation is primarily due to the

difference between calculated and measured hydrogen adsorption free energy ($\Delta G_{DFT} = -21$ kJ/mol and $\Delta G_{Exp} = -27$ kJ/mol).[54]

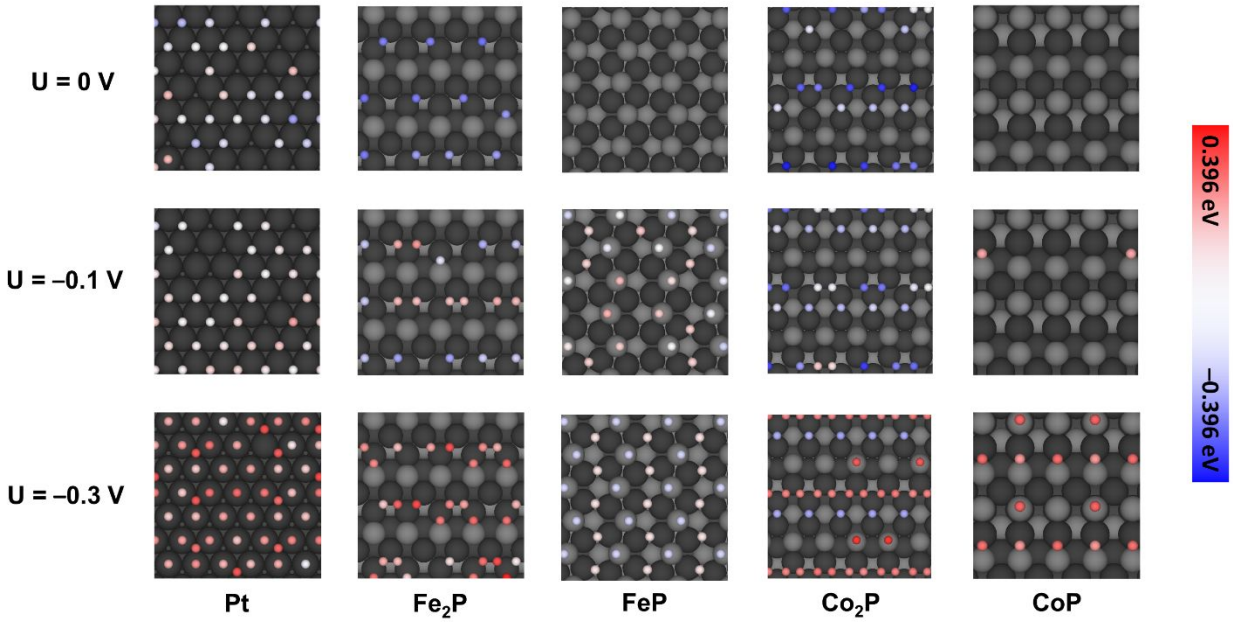

Figure 3. Snapshots of Monte Carlo simulations of adsorbed hydrogen on the surfaces of Pt(111) and phosphide surfaces. The simulations were run at 300 K with applied potentials of 0, –0.1, and –0.3 V. The grey and black spheres are the P and metal atom (Co or Fe) of the underlying material, and the colored circles represent adsorbed hydrogen atoms. The colors indicate the free energies of adsorption at each site relative to H_2. As the potential is lowered, the sites with relatively high adsorption energies start to become occupied, and these sites most readily release hydrogen to form H_2.

At 0 V, the coverage of hydrogen on CoP and FeP is significantly below that of Pt(111). The hydrogen coverage on Co_2P/Fe_2P increases more quickly than it does on CoP as the potential drops (Figure 2b). An inspection of snapshots of the Monte Carlo simulations (Figure 3) reveals that the metal-metal bridge sites on Co_2P and Fe_2P, which do not exist on CoP and FeP, are populated first. This is consistent with the stronger calculated adsorption energies on these sites (Figure 1). On

FeP(011) the hydrogen coverage of both P sites and Fe-Fe sites quickly saturate to 1 ML at around –0.1 V (Figure 2c), which suggests a phase transition with either an empty surface or a fully occupied surface being energetically favorable. This is verified by our DFT calculations of the training data, where the formation energies (with respect to an empty surface and a fully occupied surface) are positive for all intermediate hydrogen coverages (Figure S2).

For Pt(111), there is relatively little interaction between the adsorbed hydrogen atoms at low overpotentials (Figure 3), resulting in nearly uniform free energies of adsorption for all hydrogen atoms until the potential reaches –0.18 V, where a phase transition of hydrogen adsorption from the fcc site to the top site is observed (Figure S3). This phase transition was also seen in cluster expansion simulations by Tan *et al.* at a potential of about –0.4 V.[25] The differences between the two results are likely due to differences in slab thicknesses and cluster expansion parameters. Experiments also suggested that top H* appears at negative potentials after a monolayer of fcc sites are filled.[1, 56, 57]

In general, as hydrogen coverage increases the hydrogen-hydrogen lateral interactions weaken the adsorption energies of hydrogen atoms on the different surfaces, facilitating H_2 formation. This is apparent on the metal-metal bridge sites on Fe_2P and Co_2P (Figure 3), where hydrogen binding to the surface becomes notably weaker as the potential becomes more negative and coverage increases. These lateral interactions serve to enhance the activities of these sites at negative potentials relative to what would be expected based on the adsorption energy for an isolated hydrogen atom. Similarly, the higher-energy sites that are not highly occupied at 0 V become the most active ones at more negative potentials, e.g. the Pt-top sites.

We have evaluated both Volmer-Tafel and Volmer-Heyrovsky mechanisms for the HER on transition metal phosphide surfaces and Pt(111). The Volmer-Tafel mechanism involves a proton and electron transfer followed by H_2(g) chemical desorption:

$$2(H^+ + e^-) \longleftrightarrow 2H^* \longleftrightarrow H_2(g) \quad (5)$$

where 2H* denotes two adsorbed nearby hydrogen on the catalyst surface. The Volmer-Heyrovsky mechanism consists of a coupled proton-electron transfer and electrochemical desorption process:

$$H^+ + e^- \longleftrightarrow H^*, \;\; H^+ + e^- + H^* \longleftrightarrow H_2(g) \quad (6)$$

An illustration of the above elementary reaction steps (for Pt and FeP) is shown in Figure S7. The calculated free energies of adsorption on different sites and Monte Carlo snapshots (Figure 3) on the different surfaces indicate that the Volmer-Heyrovsky mechanism (or a mixed mechanism) is more likely to be predominant on transition metal phosphides than on Pt(111), due to the greater differences in hydrogen adsorption energies at neighboring sites and the increased likelihood of finding isolated hydrogen atoms with near-optimal hydrogen adsorption free energies.

To identify pairs of neighboring atoms that could desorb via the Volmer-Tafel mechanism, we have identified sites that share a common edge on a two-dimensional Voronoi diagram (Figure S8).[58] As there is a possibility that the migration of an atom from one site to another is the rate-limiting step, we have also calculated the activation barriers for diffusion between neighboring adsorption sites. The calculated activation barriers for diffusion are below the Tafel barriers, and thus it is unlikely that the surface diffusion is rate limiting. We found patterns of particularly low diffusion barriers along the metal-metal bridge (Co_2P and Fe_2P) and metal-P bridge (CoP) sites,

which are predicted to be among the most active sites on these surfaces. The maximum diffusion barrier for CoP is the lowest (~0.3 eV) among the four transition metal phosphides, which might originate from their weaker hydrogen adsorption energies.

Tafel plots (overpotential vs. log current) are commonly used to understand electrode kinetics and reaction mechanisms, and the slopes of these plots (Tafel slopes) provides insight into the reaction mechanism that allows for direct comparison between experiments and calculations.[59, 60] Across the five surfaces, we predict Tafel slopes of 32~46 mV/dec assuming the rate-limiting step is a Tafel reaction or 44~123 mV/dec assuming the rate-limiting step is a Heyrovsky reaction, which are in agreement with literature values.[9-11, 20, 61, 62] For Pt(111), the HER is favored through the Volmer-Tafel mechanism (Figure 4a) which has been suggested by experiments.[1, 63] This is primarily because the Tafel reactions have lower barriers than the Heyrovsky reactions, which is the opposite of what is observed on the phosphide catalysts. The most active sites are the Pt top sites, for which there are two possible routes (top+top or top+fcc) for the HER. The top+fcc route is more favorable due to the balance of hydrogen coverage and activation barrier. The top+top Tafel route produces a ~30 mV/dec Tafel slope, as the coverage of both of the weakly adsorbed top H* can change exponentially with applied potential. The top+fcc route has a higher Tafel slope (38 mV/dec) due to nearly saturated fcc sites, which are consistent with Lindgren *et al*.[64] The role of kinetically active Pt-top H* is in agreement with both experiments[1, 57] and simulations[25, 64].

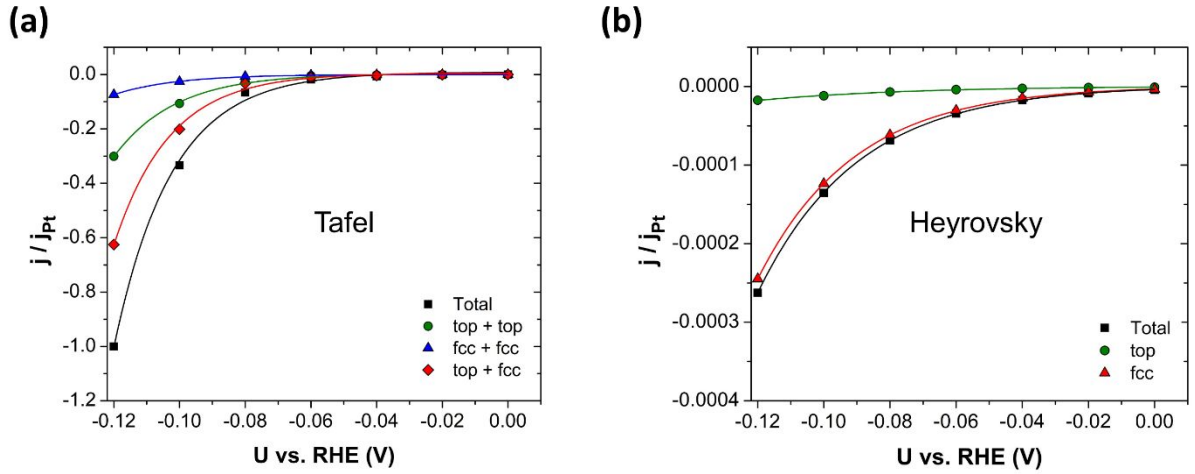

Figure 4. HER current density of Pt(111) as a function of applied potential assuming the rate-limiting step is either a Tafel reaction (a), or a Heyrovsky reaction (b). The current density is expressed as relative current to the Tafel current of Pt(111) at –0.12 V, which is denoted as j_{Pt}.

Table 1. Predicted Tafel slopes (in mV/dec) at low overpotentials (U > –0.2 V) for the Volmer-Tafel mechanism and the Volmer-Heyrovsky mechanism on transition metal phosphides and Pt, and compared with experiments.

	Tafel	Heyrovsky	Experiments	Refs.
Fe_2P	37	123	52~80	65-67
FeP	32	60	29~76	10, 65, 68
Co_2P	46	85	45~101	69-71
CoP	38	55	50~70	62, 70, 72
Pt	34	44	26~32	8, 65, 73
Ni_xP_y	/	/	27~51	9, 74, 75

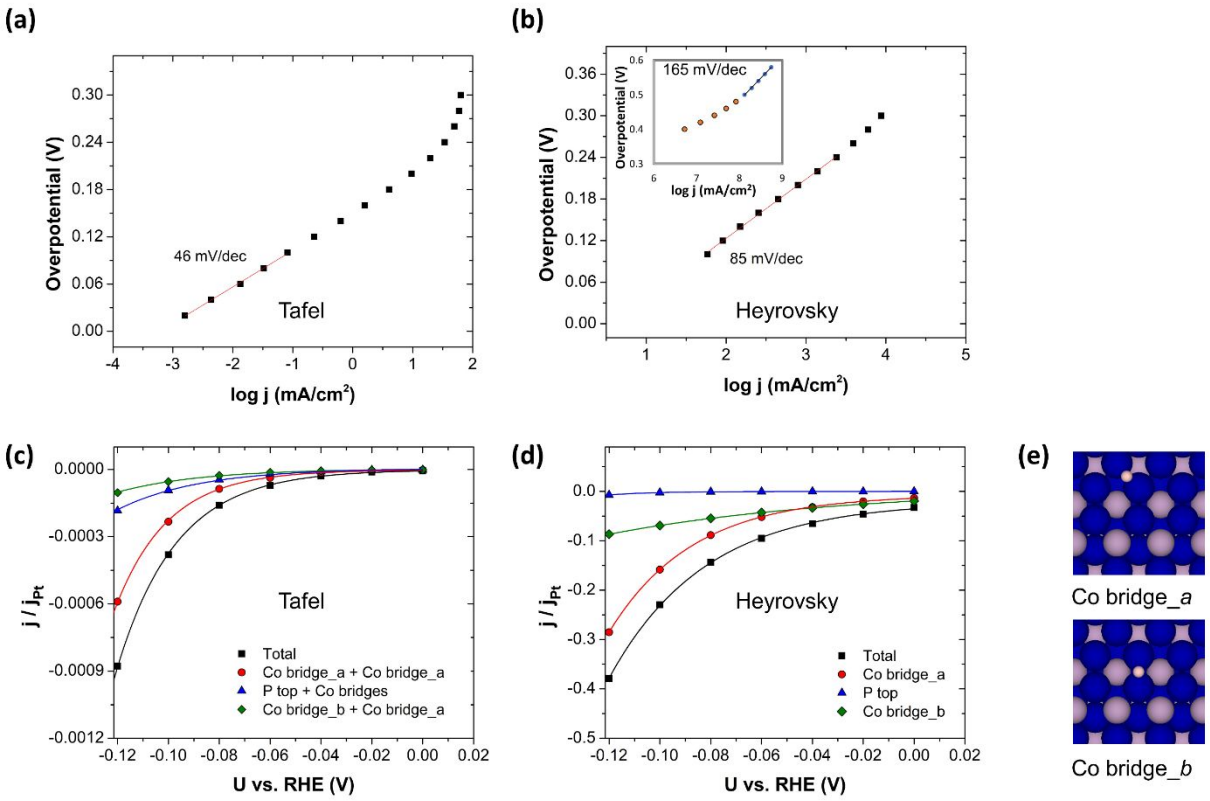

Figure 5. Tafel plots of HER on $Co_2P(101)$ assuming the rate-limiting step is either a Tafel reaction (a), or a Heyrovsky reaction (b). The inset in (b) shows the Tafel slope at higher overpotentials. Current density of $Co_2P(101)$ as a function of applied potential assuming the rate-limiting step is either a Tafel reaction (c), or a Heyrovsky reaction (d). The current density is expressed as relative current to the Tafel current of Pt(111), which is denoted as j_{Pt}. (e) Two types of Co bridge sites: "bridge_*a*" represents bridge site along *a*-axis and "bridge_*b*" represents bridge site along *b*-axis.

For CoP and FeP, the predicted Tafel slopes fall in the range of experimentally-determined values (Table 1) assuming the Heyrovsky mechanism. This slope can be understood by their dilute hydrogen coverage near 0 V so that the coverage can vary exponentially with applied potential. For Co_2P, we predict that the Tafel slope assuming the Volmer-Tafel mechanism is 46 mV/dec at low overpotentials, and transitions to infinity at high overpotentials as the surface becomes saturated (Figure 5a), which is consistent with both experiment[63] and simulation.[61] For the Volmer-

Heyrovsky mechanism, the slope is predicted to be 85 mV/dec at low overpotentials (Figure 5b) due to the partial surface coverage at 0 V and increases to 165 mV/dec at high overpotentials ($U < -0.5$ V). The Tafel slope is indeed coverage-dependent, which can be seen from our simulations (generally larger Tafel slopes) and recent studies using micro-kinetic models.[61, 76, 77] The significant increase of Tafel slope at high overpotentials can be rationalized by the loss of potential dependence of the Volmer step when all surface sites saturate.[61, 76] A theoretical value of 120 mV/dec is achieved assuming that the charge transfer coefficient is 0.5; the Tafel slope according to our Monte Carlo simulations corresponds to a charge transfer coefficient of 0.36, which is consistent with our DFT-calculated value of 0.34 (Figure S6). Similar conclusions regarding the coverage effect can be drawn for Fe_2P.

The active sites for the HER can be identified by the partial current density contributed from different types of adsorption sites. For CoP, the Tafel current is small (Figure S9a) due to low hydrogen coverage, and there is little chance of finding two neighboring hydrogen atoms (Figure 3) at low overpotentials. Therefore, the Volmer-Heyrovsky mechanism is favored. We find an anomalously low charge transfer coefficient for the P site compared to the Co site (Figure S6), which results in a lower activity for the P site at more negative potentials. The Co-P bridge sites are predicted to be the active sites for the HER on CoP (Figure S9b).

The predicted HER current densities for Co_2P as a function of applied potential assuming the rate-limiting step is either a Tafel or a Heyrovsky reaction are shown in Figure 5c and Figure 5d. The most active sites are Co-bridge sites via the Volmer-Heyrovsky mechanism, which is favored over the Volmer-Tafel mechanism by more than two orders of magnitude. This is owing to the smaller activation barriers via the Heyrovsky step than the Tafel step (by about 0.3 eV, Figure S4-S5). There are strong lateral interactions between the hydrogen atoms adsorbed on Co bridge_*a* sites (Figure 5e) that significantly weaken the hydrogen adsorption energies and facilitate H_2 evolution as coverage is increased (by lowering the activation barrier). As a result, the Tafel slope on the Co bridge_*a* site (83 mV/dec) is lower than that of the Co bridge_*b* site (185 mV/dec) at low overpotentials, and we observe a change in active sites from the Co bridge_*b* site to Co bridge_*a* site at about –0.06 V even though the hydrogen adsorption free energy for an isolated adsorbate is closer to 0 eV on the bridge_*b* site.

The trends of Tafel slope and current-voltage plot for Fe_2P resemble that of Co_2P, as they share common features of strongly adsorbed neighboring hydrogen atoms on the metal-metal bridge sites and the lateral interactions of these hydrogen atoms weaken the adsorption energy and facilitate hydrogen evolution. The calculated Tafel slope is slightly higher for Fe_2P (Table 1) than other phosphide catalysts, which results from the lower charge transfer coefficient on the metal site of Fe_2P (Figure S6). We predict that the Fe-Fe bridge sites are the most active sites (Figure S10) through the Volmer-Heyrovsky mechanism, however the mixed mechanism is possible since the Tafel current density is comparable to the Heyrovsky current density.

On FeP, the partial current density involving hydrogen bound on P-top sites remains relatively small as the potential is decreased (Figure 6a and Figure 6b) for two reasons. The first is due to

the previously-discussed low charge transfer coefficient on the P site compared to Fe site (Figure S6). The second is that we found that hydrogen adsorbed on these sites becomes more strongly bound as coverage is increased. This unusual decrease of ΔG_H at higher coverages on the P-top site was also observed by Kibsgaard *et al*.[3] We have done DFT calculations to verify that this stabilization occurs, finding that ΔG_H changes from 0.11 eV at dilute coverage to –0.06 eV at full coverage, consistent with the trend predicted by the cluster expansion. The decrease in ΔG_H with respect to coverage manifests itself in a dramatic way at about –0.1 V, at which point the previously-mentioned surface phase transformation occurs. As the potential is decreased incrementally, the hydrogen coverage jumps from nearly 0 to nearly 1 (Figure 2). At this point the Tafel current almost immediately saturates, and the Heyrovsky current jumps considerably (Figure 6) as the free energy of adsorption for both sites shifts closer to 0. The Fe-bridge sites are identified to be the most active sites for the HER on FeP (Figure 6b).

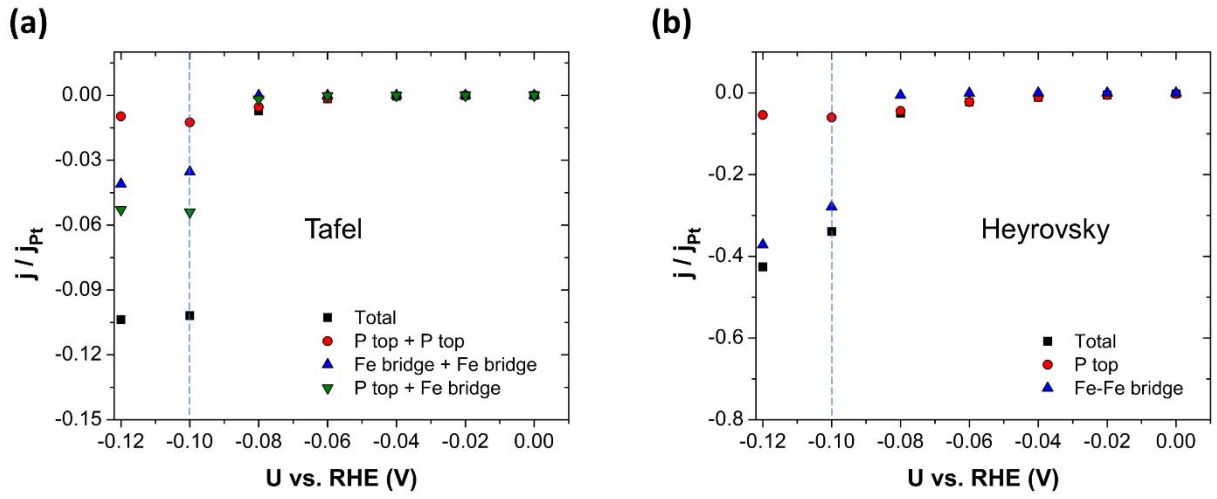

Figure 6. HER current density of FeP(011) as a function of applied potential assuming the rate-limiting step is either a Tafel reaction (a), or a Heyrovsky reaction (b). The current density is expressed as relative current to the Tafel current of Pt(111), which is denoted as j_{Pt}. The dashed line marks the phase transformation from an empty surface to a fully occupied surface.

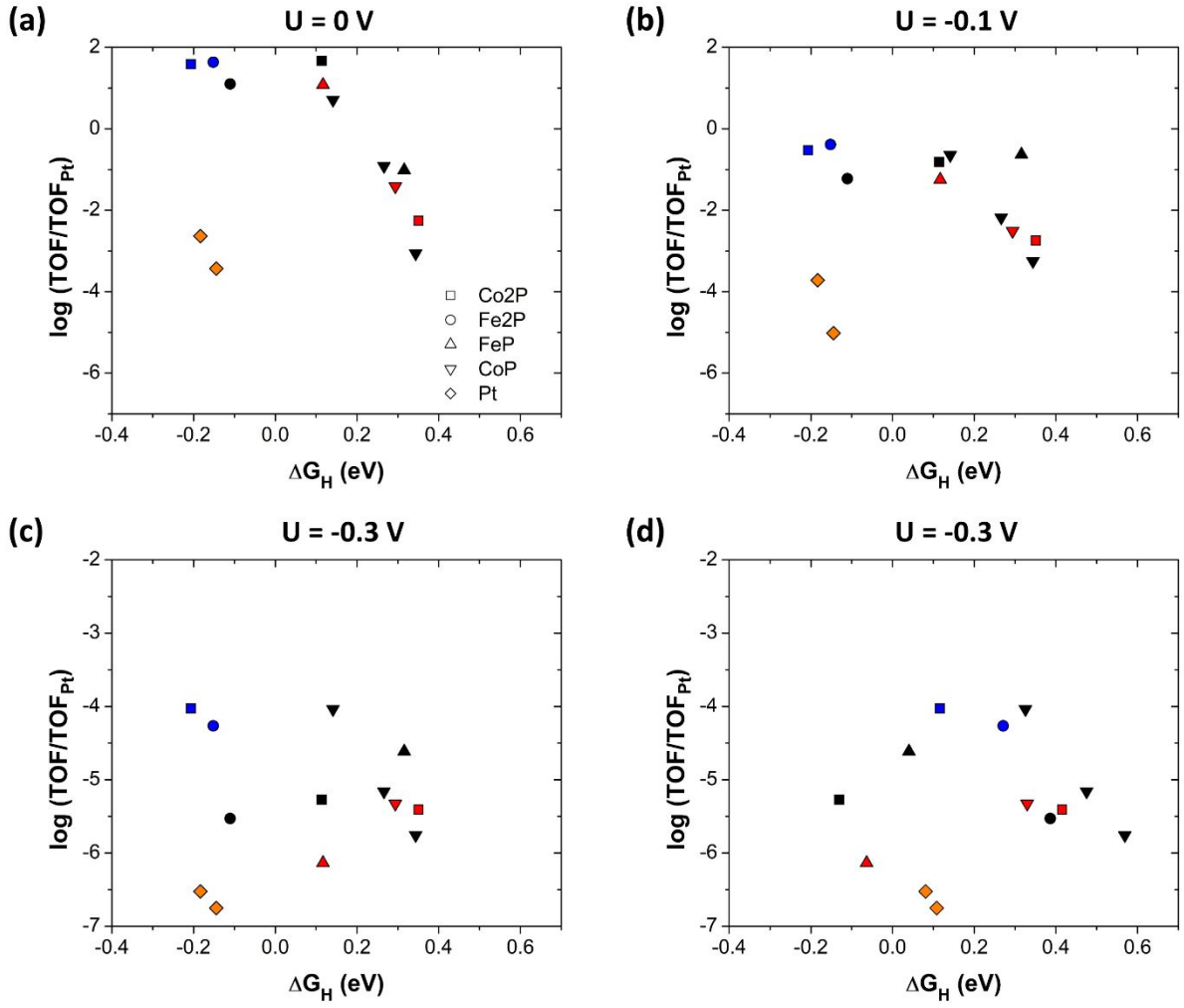

Figure 7. (a-c) Average HER (Volmer-Heyrovsky) turnover frequency (TOF) of various surface sites for which the turnover frequency is non-negligible at 0, –0.1 and –0.3 V, as a function of ΔG_H at dilute coverage. (d) Average HER (Volmer-Heyrovsky) turnover frequency of various surface sites at –0.3 V as a function of ΔG_H at full monolayer coverage. The turnover frequencies are expressed relative to that of Tafel reaction of Pt at a given potential. Color scheme: orange – Pt sites, red – P sites, blue – metal bridge sites with strong lateral interactions, black – other metal and metal-P sites.

The use of ΔG_H as a descriptor for the HER activity can be challenging for surfaces where this value is highly coverage dependent. Here we examine the trend of Heyrovsky current density at 0, –0.1 and –0.3 V as a function of ΔG_H at dilute coverage and full coverage (Figure 7a-d) for various

surface sites on the transition metal phosphides and Pt, and we discuss several ways that the volcano trend is affected by coverage. For simplicity, we limit this discussion to the Heyrovsky reaction so that we can examine the turnover frequency of each site individually.

When plotting the log of the turnover frequency at 0 V against the free energy of adsorption in the dilute limit (Figure 7a), the right leg of the volcano follows a nearly linear trend, as these sites are lightly occupied at 0 V and are generally not close to the sites that are significantly occupied at this potential. This is apparent for CoP (down triangles), for which the occupancies of all sites are predicted to be very low at 0 V (Figure 3). The linear trend is largely missing from the left side of the volcano, as ΔG_H in the dilute limit is a less accurate approximation of the actual free energy of adsorption for these sites due to coverage effects. In particular, the sites on the left side include the metal-metal bridge sites of Co_2P/Fe_2P mentioned previously, where the lateral interaction of the adsorbed H* weakens ΔG_H and facilitates hydrogen evolution. The sites on the left side also include the top site for Pt, for which occupation is suppressed due to the occupation of nearby fcc sites. Pt also does not follow the same trend as the phosphides due to a significantly different BEP relation from the phosphides. The volcano shape is somewhat restored at –0.3 V if we plot the log of the turnover frequency against the free energy of adsorption on surface in which all sites are fully occupied (Figure 7d), as this state more closely resembles the actual surface coverage at this potential (Figure 3).

On some surfaces the coverage effect manifests itself through an increase in the strength of the surface-H bond as coverage increases. From our calculations, the fcc sites on Pt(111) have ΔG_H around –0.18 eV at dilute coverage, whereas the P-top sites on FeP(011) have ΔG_H around 0.11 eV at dilute coverage, which is closer to the top of the volcano and thus might be expected to be

more active. However, we observe that P-top sites become the least active at more negative potentials. This is in part due to the low charge transfer coefficient discussed earlier, but even if we assign the same charge transfer coefficient to the P-top sites as we do to the Pt sites, we find that the Pt sites become more active as the potential is decreased due to the stabilization of hydrogen (decrease in ΔG_H) as coverage increases.

Our findings provide some insight into the design of transition metal phosphides and related catalysts. We find that the Volmer-Heyrovsky (or mixed) mechanism is more likely than the Volmer-Tafel mechanism on transition metal phosphides, in good agreement with experimental work listed in Table 1. Due to the low calculated charge transfer coefficient on phosphorous, our calculations suggest that the Heyrovsky reaction is likely to be strongly preferred at sites involving a metal atom. This is consistent with a recent experimental and computational study showing that the Fe-rich phosphide Fe_3P has a smaller Tafel slope and higher activity compared to Fe_2P and FeP, where the metal sites were found to be the most likely active sites.[65] We find that hydrogen adsorption is most likely to occur at bridge sites, and particularly favorable repulsive interactions were observed on Co_2P, for which the bridge sites are about 2.4 Å apart. As a result, of the four different model surfaces studied here, we predict the Co_2P surface to be one of the most active at low overpotentials. Considering the low surface diffusion barriers and similar adsorption energies between these active bridge sites, it may be possible to design a catalyst for which these sites are highly active via the Tafel reaction, as on Pt.

Conclusions

On transition metal phosphides, we find that sites involving metal atoms are more likely than P sites to be highly active at more negative potentials due to a low charge transfer coefficient for P.

The catalytic activity of model transition metal phosphide surfaces is found to be strongly dependent on coverage effects in a variety of ways. Lateral repulsive interactions between hydrogen atoms adsorbed at metal-metal bridge sites on Fe_2P and Co_2P surfaces significantly enhance their predicted turnover frequencies above what would be predicted by the adsorption energy of an isolated hydrogen atom. On the P site of the FeP surface, we find that the adsorbed hydrogen atom becomes more strongly bound as coverage increases, and there is a predicted phase transformation among the adsorbed hydrogen atoms at –0.1 V that leads to discontinuous jumps in coverage and catalytic activities. It is not clear whether such a phase transformation, predicted here on a model surface, appears in real-life catalysts. However the potential for such a transformation to occur is important to keep in mind for surfaces on which catalytic activity appears to be suppressed because adsorbate binding becomes stronger as coverage increases. Once the phase transformation occurs, such surfaces may become highly active.

Corresponding Author

*E-mail: tmueller@jhu.edu

Author Contributions

T.M. conceived and managed the project. H.G., W.W. and C.L. constructed the cluster expansions and calculated Tafel barriers. C.L. calculated Heyrovsky barriers and charge transfer coefficients, ran Monte Carlo simulations, and performed the analysis of coverages, Tafel slopes and current densities. C.L. and T.M. wrote the manuscript. All authors have given approval to the final version of the manuscript.

Conflicts of Interest

The authors declare no competing financial interest.

Acknowledgement

This work was supported by the Office of Naval Research through award N00014-16-1-2355. T.M., C.L., H.G., and W.W. acknowledge the computational resources provided by XSEDE through award DMR-140068 and by the Maryland Advanced Research Computing Center (MARCC). The authors also thank Georg Kastlunger, Per Lindgren, and Prof. Andrew Peterson for helpful discussions. Atomic-scale structural images were generated using VESTA.[78]

References

1. N. M. Marković, B. N. Grgur and P. N. Ross, *The Journal of Physical Chemistry B*, 1997, **101**, 5405-5413.
2. J. K. Nørskov, T. Bligaard, A. Logadottir, J. R. Kitchin, J. G. Chen, S. Pandelov and U. Stimming, *J. Electrochem. Soc.*, 2005, **152**, J23-J26.
3. J. Kibsgaard, C. Tsai, K. Chan, J. D. Benck, J. K. Norskov, F. Abild-Pedersen and T. F. Jaramillo, *Energy & Environmental Science*, 2015, **8**, 3022-3029.
4. E. J. Popczun, C. G. Read, C. W. Roske, N. S. Lewis and R. E. Schaak, *Angew. Chem.*, 2014, **126**, 5531-5534.
5. E. J. Popczun, J. R. McKone, C. G. Read, A. J. Biacchi, A. M. Wiltrout, N. S. Lewis and R. E. Schaak, *J. Am. Chem. Soc*, 2013, **135**, 9267-9270.
6. Y. Zheng, Y. Jiao, M. Jaroniec and S. Z. Qiao, *Angew. Chem. Int. Ed.*, 2015, **54**, 52-65.
7. M. H. Hansen, L.-A. Stern, L. Feng, J. Rossmeisl and X. Hu, *PCCP*, 2015, **17**, 10823-10829.
8. C. Tang, L. Gan, R. Zhang, W. Lu, X. Jiang, A. M. Asiri, X. Sun, J. Wang and L. Chen, *Nano Lett.*, 2016, **16**, 6617-6621.
9. A. B. Laursen, K. R. Patraju, M. J. Whitaker, M. Retuerto, T. Sarkar, N. Yao, K. V. Ramanujachary, M. Greenblatt and G. C. Dismukes, *Energy & Environmental Science*, 2015, **8**, 1027-1034.
10. X. Yang, A.-Y. Lu, Y. Zhu, S. Min, M. N. Hedhili, Y. Han, K.-W. Huang and L.-J. Li, *Nanoscale*, 2015, **7**, 10974-10981.
11. J. Tian, Q. Liu, Y. Liang, Z. Xing, A. M. Asiri and X. Sun, *ACS Applied Materials & Interfaces*, 2014, **6**, 20579-20584.
12. D. Zhou, L. He, W. Zhu, X. Hou, K. Wang, G. Du, C. Zheng, X. Sun and A. M. Asiri, *Journal of Materials Chemistry A*, 2016, **4**, 10114-10117.
13. R. Parsons, *Transactions of the Faraday Society*, 1958, **54**, 1053-1063.
14. J. Greeley, T. F. Jaramillo, J. Bonde, I. Chorkendorff and J. K. Norskov, *Nat Mater*, 2006, **5**, 909-913.
15. A. B. Laursen, R. B. Wexler, M. J. Whitaker, E. J. Izett, K. U. D. Calvinho, S. Hwang, R. Rucker, H. Wang, J. Li, E. Garfunkel, M. Greenblatt, A. M. Rappe and G. C. Dismukes, *ACS Catal.*, 2018, **8**, 4408-4419.
16. R. B. Wexler, J. M. P. Martirez and A. M. Rappe, *ACS Catal.*, 2017, **7**, 7718-7725.
17. E. Skúlason, V. Tripkovic, M. E. Björketun, S. Gudmundsdottir, G. Karlberg, J. Rossmeisl, T. Bligaard, H. Jónsson and J. K. Nørskov, *J. Phys. Chem. C*, 2010, **114**, 18182-18197.
18. C. Tsai, K. Chan, J. K. Nørskov and F. Abild-Pedersen, *Catalysis Science & Technology*, 2015, **5**, 246-253.
19. Y. Shao, X. Shi and H. Pan, *Chem. Mater.*, 2017, **29**, 8892-8900.
20. S. Anantharaj, S. R. Ede, K. Sakthikumar, K. Karthick, S. Mishra and S. Kundu, *ACS Catal.*, 2016, **6**, 8069-8097.
21. E. Ising, *Zeitschrift für Physik*, 1925, **31**, 253-258.
22. J. M. Sanchez, F. Ducastelle and D. Gratias, *Physica A: Statistical Mechanics and its Applications*, 1984, **128**, 334-350.
23. W. Kohn and L. J. Sham, *Physical Review*, 1965, **140**, A1133-A1138.

24. T. L. Tan, L.-L. Wang, D. D. Johnson and K. Bai, *Nano Letters*, 2012, **12**, 4875-4880.
25. T. L. Tan, L.-L. Wang, D. D. Johnson and K. Bai, *J. Phys. Chem. C*, 2013, **117**, 22696-22704.
26. T. L. Tan, L.-L. Wang, J. Zhang, D. D. Johnson and K. Bai, *ACS Catal.*, 2015, **5**, 2376-2383.
27. T. Mueller, *Physical Review B*, 2012, **86**, 144201.
28. T. Mueller and G. Ceder, *ACS Nano*, 2010, **4**, 5647-5656.
29. X. Huang, Z. Zhao, L. Cao, Y. Chen, E. Zhu, Z. Lin, M. Li, A. Yan, A. Zettl, Y. M. Wang, X. Duan, T. Mueller and Y. Huang, *Science*, 2015, **348**, 1230-1234.
30. C. Li, D. Raciti, T. Pu, L. Cao, C. He, C. Wang and T. Mueller, *The Journal of Physical Chemistry C*, 2018, **122**, 18040-18047.
31. L. Cao and T. Mueller, *The Journal of Physical Chemistry C*, 2015, **119**, 17735-17747.
32. Q. Jia, Z. Zhao, L. Cao, J. Li, S. Ghoshal, V. Davies, E. Stavitski, K. Attenkofer, Z. Liu, M. Li, X. Duan, S. Mukerjee, T. Mueller and Y. Huang, *Nano Letters*, 2018, **18**, 798-804.
33. L. Cao and T. Mueller, *Nano Letters*, 2016, **16**, 7748–7754.
34. L. Cao, C. Li and T. Mueller, *Journal of Chemical Information and Modeling*, 2018, **58**, 2401-2413.
35. F. Hess and H. Over, *ACS Catal.*, 2017, **7**, 128-138.
36. C. Wu, D. J. Schmidt, C. Wolverton and W. F. Schneider, *J. Catal.*, 2012, **286**, 88-94.
37. J. Teeriniemi, M. Melander, S. Lipasti, R. Hatz and K. Laasonen, *J. Phys. Chem. C*, 2017, **121**, 1667-1674.
38. N. Metropolis, A. W. Rosenbluth, M. N. Rosenbluth, A. H. Teller and E. Teller, *The Journal of Chemical Physics*, 1953, **21**, 1087-1092.
39. G. Kresse and J. Furthmüller, *Physical Review B*, 1996, **54**, 11169-11186.
40. B. Hammer, L. B. Hansen and J. K. Nørskov, *Physical Review B*, 1999, **59**, 7413-7421.
41. J. P. Perdew, K. Burke and M. Ernzerhof, *Phys. Rev. Lett.*, 1996, **77**, 3865-3868.
42. P. E. Blochl, *Physical Review B*, 1994, **50**, 17953-17979.
43. P. Wisesa, K. A. McGill and T. Mueller, *Physical Review B*, 2016, **93**, 155109.
44. G. Henkelman, B. P. Uberuaga and H. Jónsson, *The Journal of Chemical Physics*, 2000, **113**, 9901-9904.
45. G. Henkelman and H. Jónsson, *The Journal of Chemical Physics*, 2000, **113**, 9978-9985.
46. T. Mueller and G. Ceder, *Physical Review B*, 2009, **80**, 024103.
47. J. N. Bronsted, *Chem. Rev.*, 1928, **5**, 231-338.
48. M. G. Evans and M. Polanyi, *Transactions of the Faraday Society*, 1938, **34**, 11-24.
49. J. K. Nørskov, T. Bligaard, A. Logadottir, S. Bahn, L. B. Hansen, M. Bollinger, H. Bengaard, B. Hammer, Z. Sljivancanin, M. Mavrikakis, Y. Xu, S. Dahl and C. J. H. Jacobsen, *J. Catal.*, 2002, **209**, 275-278.
50. K. Chan and J. K. Nørskov, *The Journal of Physical Chemistry Letters*, 2015, **6**, 2663-2668.
51. J. Rossmeisl, E. Skúlason, M. E. Björketun, V. Tripkovic and J. K. Nørskov, *Chem. Phys. Lett.*, 2008, **466**, 68-71.
52. J. K. Nørskov, J. Rossmeisl, A. Logadottir, L. Lindqvist, J. R. Kitchin, T. Bligaard and H. Jónsson, *The Journal of Physical Chemistry B*, 2004, **108**, 17886-17892.
53. E. Skulason, G. S. Karlberg, J. Rossmeisl, T. Bligaard, J. Greeley, H. Jonsson and J. K. Norskov, *PCCP*, 2007, **9**, 3241-3250.

54. N. M. Marković, T. J. Schmidt, B. N. Grgur, H. A. Gasteiger, R. J. Behm and P. N. Ross, *The Journal of Physical Chemistry B*, 1999, **103**, 8568-8577.
55. B. E. Conway, H. Angerstein-Kozlowska and H. P. Dhar, *Electrochim. Acta*, 1974, **19**, 455-460.
56. N. M. Marković and P. N. Ross, *Surf. Sci. Rep.*, 2002, **45**, 117-229.
57. D. E. Ramaker and C. Roth, *ChemElectroChem*, 2015, **2**, 1582-1594.
58. F. Aurenhammer, *ACM Comput. Surv.*, 1991, **23**, 345-405.
59. J. Tafel, *Journal*, 1905, **50U**, 641.
60. Y.-H. Fang and Z.-P. Liu, *ACS Catal.*, 2014, **4**, 4364-4376.
61. T. Shinagawa, A. T. Garcia-Esparza and K. Takanabe, *Scientific Reports*, 2015, **5**, 13801.
62. L. Yang, H. Qi, C. Zhang and X. Sun, *Nanotechnology*, 2016, **27**, 23LT01.
63. K. Magdić Košiček, K. Kvastek and V. Horvat-Radošević, *J. Solid State Electrochem.*, 2016, **20**, 3003-3013.
64. P. Lindgren, G. Kastlunger and A. A. Peterson, *arXiv: 1903.09903 [physics. chem-ph]* 2019.
65. D. E. Schipper, Z. Zhao, H. Thirumalai, A. P. Leitner, S. L. Donaldson, A. Kumar, F. Qin, Z. Wang, L. C. Grabow, J. Bao and K. H. Whitmire, *Chem. Mater.*, 2018, **30**, 3588-3598.
66. H. Hu, Q. Zhang, F. Luo, L. Guo, K. Qu, Z. Yang, S. Xiao, Z. Xu, W. Cai and H. Cheng, *ChemElectroChem*, 2019, **6**, 1413-1418.
67. J. Yang, Y. Ouyang, H. Zhang, H. Xu, Y. Zhang and Y. Wang, *Journal of Materials Chemistry A*, 2016, **4**, 9923-9930.
68. Y. Liang, Q. Liu, A. M. Asiri, X. Sun and Y. Luo, *ACS Catal.*, 2014, **4**, 4065-4069.
69. Y. Zhang, L. Gao, E. J. M. Hensen and J. P. Hofmann, *ACS Energy Letters*, 2018, **3**, 1360-1365.
70. J. F. Callejas, C. G. Read, E. J. Popczun, J. M. McEnaney and R. E. Schaak, *Chem. Mater.*, 2015, **27**, 3769-3774.
71. Y. Pan, Y. Lin, Y. Chen, Y. Liu and C. Liu, *Journal of Materials Chemistry A*, 2016, **4**, 4745-4754.
72. Y.-P. Zhu, Y.-P. Liu, T.-Z. Ren and Z.-Y. Yuan, *Adv. Funct. Mater.*, 2015, **25**, 7337-7347.
73. H. Wei, H. Wu, K. Huang, B. Ge, J. Ma, J. Lang, D. Zu, M. Lei, Y. Yao, W. Guo and H. Wu, *Chemical Science*, 2019, **10**, 2830-2836.
74. A. Han, S. Jin, H. Chen, H. Ji, Z. Sun and P. Du, *Journal of Materials Chemistry A*, 2015, **3**, 1941-1946.
75. P. Jiang, Q. Liu and X. Sun, *Nanoscale*, 2014, **6**, 13440-13445.
76. A. Kahyarian, B. Brown and S. Nesic, *J. Electrochem. Soc.*, 2017, **164**, H365-H374.
77. N. P. Subramanian, T. A. Greszler, J. Zhang, W. Gu and R. Makharia, *J. Electrochem. Soc.*, 2012, **159**, B531-B540.
78. K. Momma and F. Izumi, *J. Appl. Crystallogr.*, 2008, **41**, 653-658.

TOC